Japanese Journal of Applied Physics

RAPID COMMUNICATION

Fabrication of ordered arrays of GeSn nanodots using anodic aluminum oxide as a template

To cite this article: Qiuhong Gan *et al* 2022 *Jpn. J. Appl. Phys.* **61** 070902

Japanese Journal of Applied Physics **61**, 070902 (2022) **RAPID COMMUNICATION**
https://doi.org/10.35848/1347-4065/ac759a

Fabrication of ordered arrays of GeSn nanodots using anodic aluminum oxide as a template

Qiuhong Gan[1], Jiulong Yu[1], Ye Liao[1], Wei Huang[1*], Guangyang Lin[1], Jianyuan Wang[1], Jianfang Xu[1], Cheng Li[1], Songyan Chen[1], and Jun Zheng[2]

[1]*Department of Physics, Xiamen University, Xiamen, Fujian 361005, People's Republic of China*
[2]*State Key Laboratory on Integrated Optoelectronics, Institute of Semiconductors, Chinese Academy of Sciences, Beijing 100083, People's Republic of China*

[*]E-mail: weihuang@xmu.edu.cn

Received March 19, 2022; revised April 29, 2022; accepted June 2, 2022; published online June 17, 2022

A method to grow GeSn nanodots has been developed by magnetron sputtering using anodic aluminum oxide as a template. With a high substrate temperature and a high deposition rate, flattened hill-like GeSn nanodots with high Sn content have been successfully formed directly on Ge(001) and Si(001) substrates. The GeSn nanodots are polycrystalline on Si and monocrystalline on Ge without Sn segregation. High-resolution transmission electron microscopy observations revealed that GeSn nanodots formed on Ge had a perfect interface without misfit dislocations.

Silicon photonics is a fast-growing technology that integrates photonic circuits onto a Si substrate and has been growing steadily since the 1980s.[1,2] GeSn materials have attracted much attention as a promising optoelectronic material that is compatible with Si-based CMOS processes.[3,4] GeSn have higher carrier mobilities than Si,[5] and the energy band of GeSn materials can be regulated by Sn content. When the Sn content reaches 6%–10% or more,[6,7] GeSn materials could transfer from indirect to direct bandgap. However, Sn atoms can hardly incorporate into the Ge lattice matrix caused of the large difference in lattice between Ge and Sn. Therefore, the equilibrium solid solubility of Sn in Ge is less than 1% leads to Sn segregation at high temperatures.[8–10] To overcome these difficulties, non-equilibrium methods including molecular beam epitaxy (MBE),[11–13] chemical vapor deposition (CVD),[14–16] and magnetron sputtering[17,18] are widely used for the preparation of high-quality GeSn materials with high Sn content.

On the other hand, for the obtained GeSn bulk material with high Sn content, the bandgap could be too narrow to reach the optical communication 1550 nm wavelength. GeSn nanodots could be an effective solution to enlarge the bandgap by the quantum confinement effect.[19] Several approaches have been proposed to produce GeSn nanocrystals so far, such as GeSn nanodots grown on ultrathin SiO_2 films,[20] GeSn nanodots with Sn mediation,[21] GeSn nanodots based on Sn diffusion by sputtering,[22] and so on. Aiming to obtain aligned nanodot arrays, several techniques such as multilayer stacking[23] and self-assembled porous templates[24,25] were studied. Other than the above methods, using anodic aluminum oxide (AAO) as a template was proved to be a cost-effective and convenient way to fabricate uniform nanodot arrays such as InAs,[26] GaAs,[27] and Ge.[28]

In this work, we studied the crystallization of GeSn films on Si and Ge substrates as well as GeSn nanodots with a template of AAO on Si and Ge substrates by sputtering. It is found that the GeSn films were obtained with good crystal quality at higher temperatures and deposition rates. The formed GeSn nanodots are demonstrated as polycrystalline on Si and monocrystalline on Ge, respectively. No Sn segregation was found on the surface of the GeSn dots.

Before the GeSn films and GeSn nanodots growth by magnetron sputtering, Si (001) substrates were cleaned by the RCA cleaning method, while Ge (001) substrates were cleaned with acetone, alcohol, 10% HF, and deionized water sequentially. To fabricate the GeSn nanodots, the substrates were transferred by AAO templates in acetone and then immediately loaded into the sputtering chamber. The base pressure of the sputtering chamber was better below 7×10^{-5} Pa. GeSn was then sputtered from a high purity GeSn target (99.999%) with 12 at% Sn content. During the deposition, the substrate was kept at calibrated temperatures ranging from 124 °C to 276 °C, respectively. And the ambient pure Ar gas pressure was fixed at 0.5 Pa. For GeSn films, the thickness is 300 nm. For GeSn nanodots, the nominal deposition thickness is 50 nm. The deposition rate was separately controlled from 3.3 to 25 nm min^{-1}. After GeSn deposition, the GeSn nanodots are finally obtained by detaching the AAO template simply using polyimide adhesive tape.

The surface morphology of samples was investigated by scanning electron microscopy (SEM). High-resolution transmission electron microscopy (HRTEM) and energy dispersive spectroscopy (EDS) were used to characterize the crystallinity and composition of the GeSn nanodots. For the GeSn films, Raman scattering and X-Ray diffraction (XRD) were conducted to investigate the crystalline quality.

Before the growth of the GeSn nanodots, the growth of the GeSn films was firstly studied to find the optimized deposition conditions. During film growth, the temperature is the most effective parameter to improve the materials' crystallinity, especially for GeSn. At a fixed growth rate of 8 nm min^{-1}, GeSn films were grown on Si at various temperatures. As shown by the Raman scattering spectra in Fig. 1(a), the GeSn film grown at 164 °C was amorphous while the GeSn film began to crystallize at a grown temperature of 212 °C. Further crystallization was verified by narrowing the Raman crystalline peak and shifting toward a higher wave number as the growth temperature was increased to 276 °C.

However, the (111), (220), and (311) XRD peaks showed that the GeSn film grown at the temperature of 212 °C is just polycrystalline [Fig. 1(b)]. By further increasing the growth temperature to 276 °C, the GeSn (004) XRD peak started to emerge at $\theta = 32.9°$, and the (111), (220), and (311) XRD peaks all disappeared. This indicates the epitaxially growth of GeSn on the Si(001) substrate. So the rise of the GeSn(004)

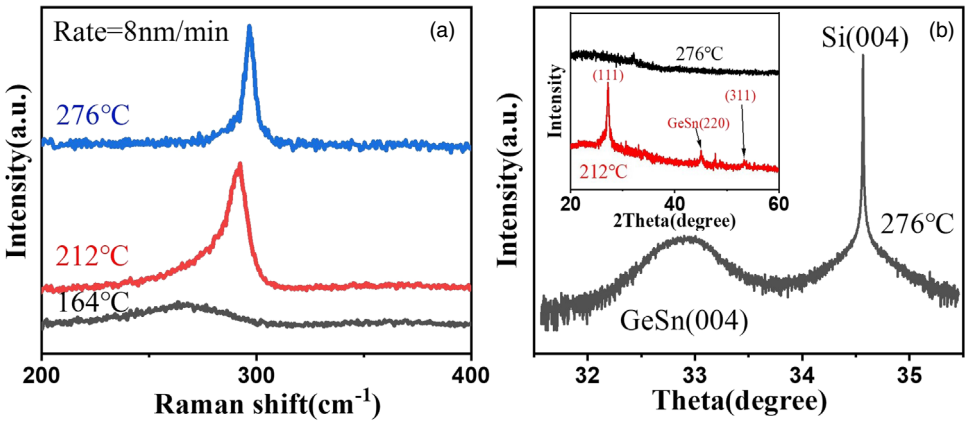

Fig. 1. (Color online) (a) Raman spectra of GeSn films grown on Si(001) at different temperatures (T). (b) XRD scan of GeSn film grown on Si(001) at 276 °C, the deposition rate (Rate) is 8 nm min^{-1}. The inset shows the XRD scans from $2\theta = 20°$ to 60° of the two crystalline samples in (a).

XRD peak can be regarded as a symbol of monocrystalline GeSn formation.

The crystallinity of the GeSn film is also affected by the deposition rate. To investigate the effect of deposition rate, the growth temperature was fixed at 276 °C and the deposition rate varied from 3.3 to 25 nm min^{-1} during the sputterings. As shown in Fig. 2(a), with increasing deposition rate, the GeSn (004) peak is found to move to a lower degree presenting enhanced Sn content incorporation. Our GeSn films are 300 nm thick in their thicknesses, the strain of the GeSn films is assumed to all be relaxed. Maintaining the deposition rate of 25 nm min^{-1}, the temperature was carefully tuned within a small window between 250 °C and 276 °C. The monocrystallinity is found very sensitive to the growth temperature as shown by the XRD patterns in Fig. 2(b). As the growth temperature was reducing, the GeSn(004) peak quickly disappeared which indicated the transformation between polycrystalline and monocrystalline. As concluded from the above results, epitaxial growth of GeSn is favored by a relatively higher growth temperature and growth rate. Due to the limitation of our equipment, even higher growth temperature and faster growth rate are not possible.

The rapid deposition rate is regarded to reduce Sn surface segregation and increase Sn incorporation as more Sn atoms are immediately buried into the Ge lattice matrix before segregation. And high Sn content in GeSn leads to a lower nucleation potential barrier for GeSn crystallization and improved film crystallinity.[22] Such a Sn migration model predicted a uniform high Sn content depth distribution in the GeSn film and improved film crystallinity as verified by the MBE GeSn layer growth work of Noriyuki et al.[29] Improved

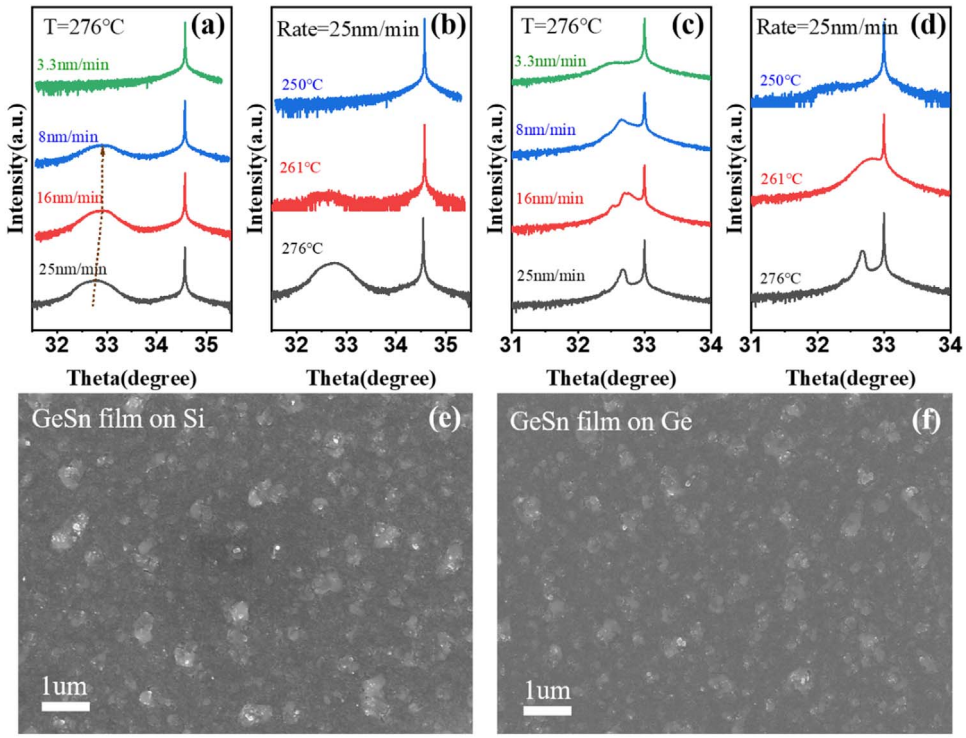

Fig. 2. (Color online) XRD scans of GeSn films grown on Si(001) (a) with various deposition rates (Rate) and a fixed growth temperature (*T*) of 276 °C and (b) with various growth temperatures at a fixed deposition rate of 25 nm min^{-1}. XRD scans of GeSn films grown on Ge(001) (c) with various deposition rates and a fixed *T* of 276 °C and (d) with various growth temperatures and a fixed rate of 25 nm min^{-1}. SEM images of Sn segregation on the surface of GeSn films grown at 276 °C and 25 nm min^{-1} on Si and Ge, respectively (e), (f).

crystallinity of the GeSn films with a high deposition rate was also reported for CVD method[30] and a magnetron sputtering method.[31]

The growth of GeSn film on Ge is also performed. Both the growth temperature and the deposition rate are studied to show their effect on the crystallinity of the GeSn film. A similar conclusion can be drawn which gave the best growth condition of 276 °C and 25 nm min^{-1}. But it seems that the formed GeSn film acquired much-improved monocrystallinity on Ge since the lattice mismatch between GeSn and Ge is much smaller than that between GeSn and Si. As indicated in Figs. 2(c) and 2(d), narrower and stronger (004) XRD peaks were recorded for the GeSn films grown on Ge when using the same growth condition as that grown on Si. Although a fast deposition rate was employed to improve the film crystallinity, serious Sn surface segregation was still observed for the GeSn films grown on Si and Ge at 276 °C and 25 nm min^{-1} as shown in Figs. 2(e) and 2(f). Therefore, relatively low Sn contents of the two films were calculated to be 4.6 and 6.1 at% by Vegards' law and the estimated GeSn lattice parameters from the GeSn(004) XRD peaks.

With the same sputtering technique and by using AAO as the template, GeSn nanodots were formed on Si and Ge substrates. SEM morphologies of the GeSn nanodots formed on Si(001) at 8 nm min^{-1} with various growth temperatures (124 °C–276 °C) are shown in Fig. 3. The average diameter of 70 nm of the nanodots matches the pore size of the AAO templates. The density of GeSn nanodots was 7.4×10^9 cm^{-2}. By replacing the AAO template, smaller nanodots down to 30 nm and higher dot density up to 10^{10} cm^{-2} could also be realized. The surfaces of the GeSn nanodots were smooth when grown at 124 °C and 164 °C. With a higher growth temperature of 212 °C, the GeSn nanodots started to show the morphology of many nano-bulges. When the temperature reaches 276 °C, the surface bulges of GeSn nanodots became even larger as seen in Fig. 3(d). Comparing the morphology evolution and the Raman crystallinity analysis in Fig. 1, the rough bulge-like surface morphology is ascribed to the crystallization of the nanodots.

Cross-section TEM of the GeSn nanodots grown at 276 °C and 8 nm min^{-1} is shown in Figs. 4(a) and 4(b). The nanodots are comprised of several large grains with random crystal orientation. The interfaces between the grains and the Si substrate are disturbed. EDS mapping (not shown) also reviewed oxygen contaminations at the grain/Si interfaces. The deposition condition of the polycrystalline GeSn nanodot in Fig. 4(b) has been controlled exactly the same as for the monocrystalline GeSn film grown on Si in Fig. 1(b). However, the GeSn nanodots failed to epitaxially grow on Si(001). It is noticed that the maximum height of the GeSn nanodots is only 25 nm. Compared to the nominal deposition thickness of 50 nm, the actual deposition rate of the GeSn nanodots is almost half of the blanket deposition rate due to the shadowing effect.[32] Probably, the lowered deposition rate caused the failure of the epitaxial growth. To improve GeSn nanodots' crystal quality on Si, the deposition rate is further increased to 25 nm min^{-1} with the same 276 °C growth temperature. As can be seen in Fig. 4(c), the surface morphology of nanodots did not change after the deposition rate was increased. Although the size of the grain has become almost as large as the whole dot as seen in Fig. 4(d), quantities of tiny grains and oxygen contaminations were still observed at the GeSn/Si interface, which indicated the tremendous difficulty of the GeSn epitaxy on Si.

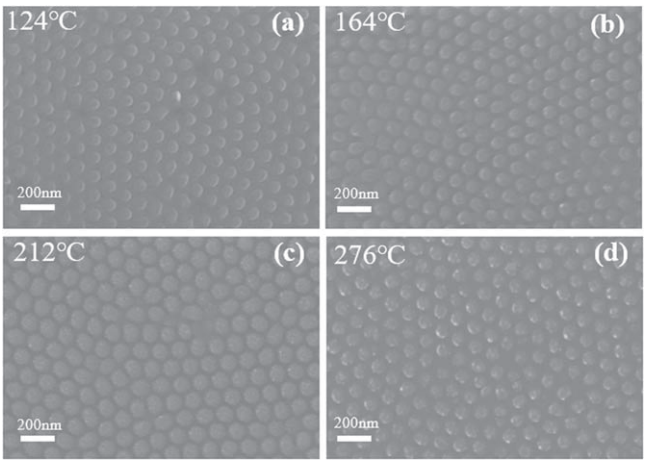

Fig. 3. (a)–(d) SEM images of GeSn nanodots formed on Si(001) substrate with various growth temperatures. The deposition rate is fixed at 8 nm min^{-1}.

GeSn nanodots were also grown on Ge(001) substrates. At a first sight, the GeSn nanodots showed a somewhat rectangle shape which is obviously different from the round shape of the AAO pores as seen in Fig. 5(a). Further HRTEM study in Fig. 5(b) showed that nanodots comprising high-quality GeSn single-crystal grains are observed epitaxially grown on the Ge substrate. The lattice alignment across the GeSn/Ge interface is perfect without any obvious mismatch defect. As a consequence, the interface became almost invisible in Fig. 5(c). Figure 5(d) shows the inverse fast Fourier transform (IFFT) figure across the GeSn/Ge interface. The extracted atomic (111) planes across the interface are verified to be intact without any fracture or broken end.

EDS elemental analysis in Fig. 5(e) showed that the Sn element was distributed uniformly in the GeSn nanodot. An EDS line scan in Fig. 5(f) showed that the Sn content in GeSn nanodot grown on Ge reached as high as 16 at%. Compared to the 12 at% Sn content in the GeSn target, the higher Sn content in the nanodot came from the higher sputtering yield of Sn over Ge. Another possible reason is ascribed to the serious surface Sn segregation of the GeSn sputtering target. Anyhow, the Sn segregation is not observed in the fabricated GeSn nanodots even if its Sn content has reached so high. As compared to the serious Sn segregation in the GeSn films with the final Sn content of 4.6–6.1 at%, nanodots show the great potential to incorporate more Sn content. As is known, extremely low solid solubility (<1%) of Sn in Ge came from the large difference in atoms' size (14.6%) between the two atoms. But for nano-structured GeSn material, the high surface-to-volume ratio provides more free surface sites to relax the local lattice matrix strain and accommodate higher Sn content. With the nano-structured GeSn, the Sn content can easily reach over 10 at% as shown by our previous work and many other reports.[21,22,33] Such a high Sn content in our GeSn nanodots is obviously higher than the reported GeSn nanodots grown by Stranski–Krastanov growth mechanism on Si[34] and the GeSn nanodots array fabricated by Nanoheteroepitaxy technology.[35] Our Sn content is also comparable to the high 13% Sn content of the GeSn nanodots

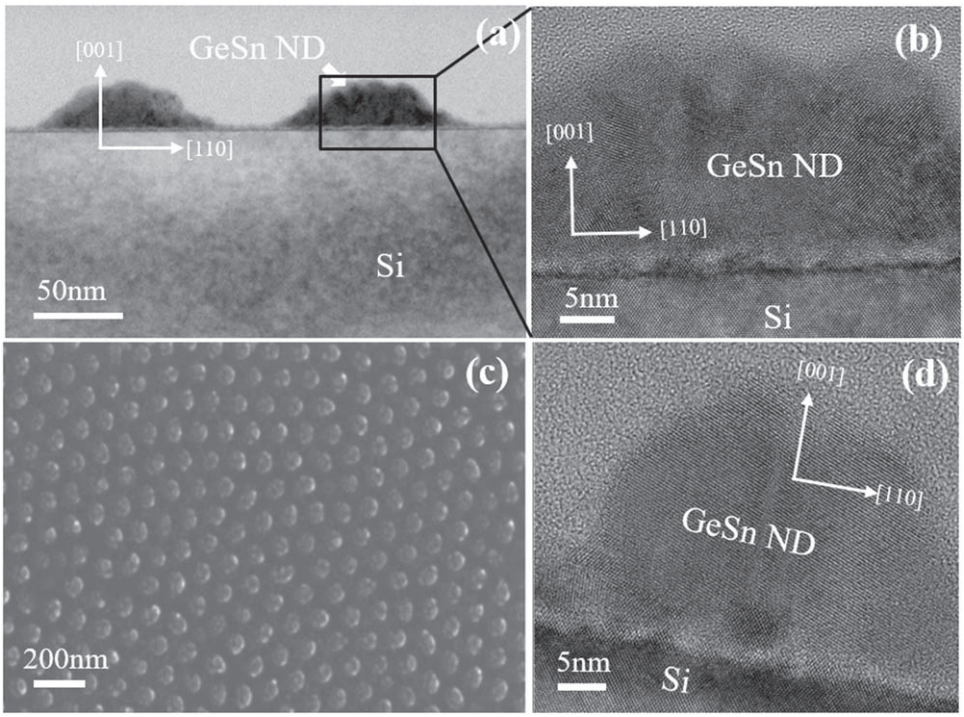

Fig. 4. GeSn nanodots grown on Si(001) with a growth temperature of 276 °C and a deposition rate of 8 nm min^{-1}: (a) TEM image, (b) HRTEM image. GeSn nanodots grown on Si(001) with a growth temperature of 276 °C and an increased deposition rate of 25 nm min^{-1}: (c) SEM image, (d) HRTEM image.

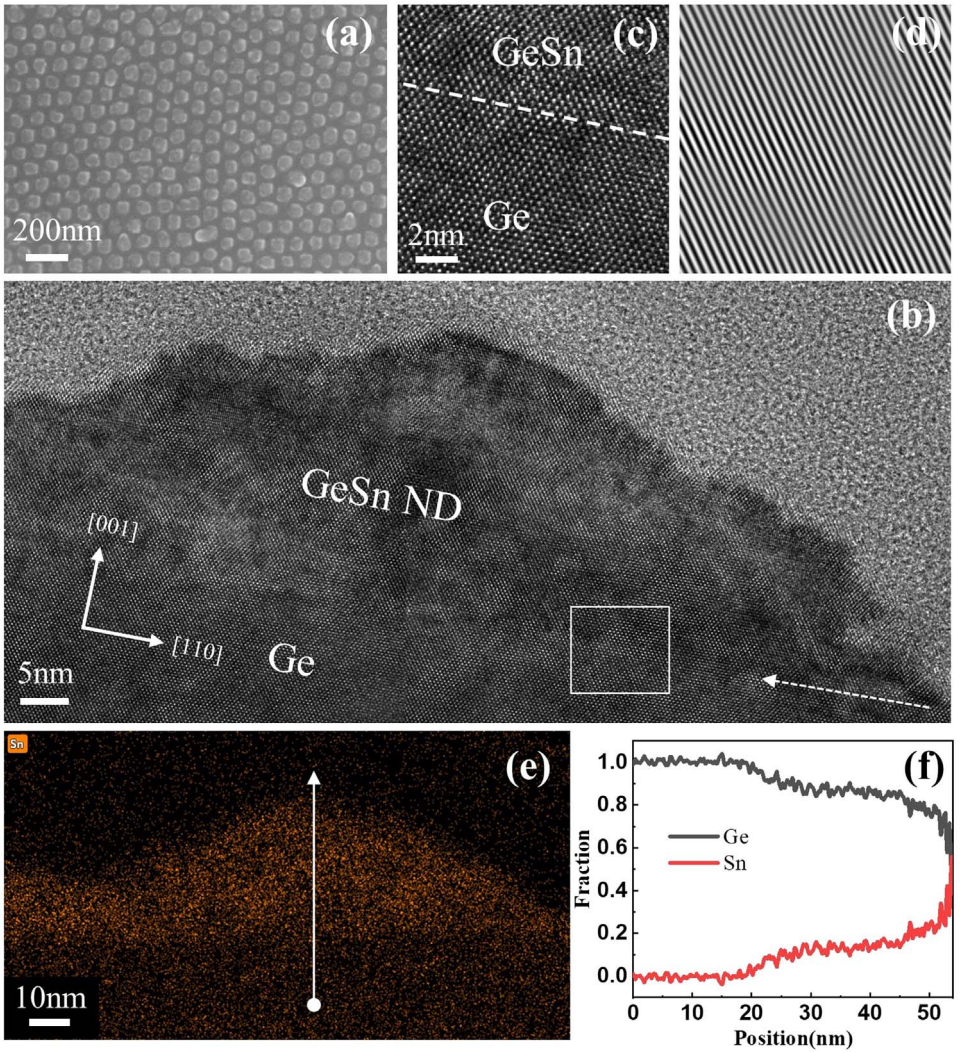

Fig. 5. (Color online) GeSn nanodots grown at 276 °C and 25 nm min^{-1} on Ge(001). (a) SEM image. (b) HRTEM image of one GeSn nanodot. the white dot arrow indicates the position of the GeSn/Ge epitaxial interface. (c) magnified image of the white rectangle in (d) which corresponds to a region of the GeSn/Ge interface. (d) IFFT pattern of (c). (e) EDS mapping of Sn element. (f) EDS line scan of Ge and Sn follow the white arrow in (e).

fabricated by MBE combined with nano-SiO_2 template.[20] The high Sn content in GeSn nanodots favors the fulfillment of the direct-band GeSn material which can be employed in Si photonics. As a future work, optical characterization of the GeSn nanodots is be carried out.

In summary, high Sn fraction (∼16%) nanodots monocrystalline GeSn nanodots with a uniform size of 70 nm were successfully fabricated by magnetron sputtering on Ge(001) with a growth temperature of 276 °C and a deposition rate of 25 nm min^{-1}. The GeSn nanodots epitaxially grown on Ge exhibited a high-quality interface without misfit defects. For GeSn nanodots grown on Si, polycrystalline structure was formed composed of several grains without epitaxy due to the oxygen contaminations and large lattice mismatch between GeSn and Si. The Sn atoms were uniformly distributed in all GeSn nanodots without any observable segregation.

Acknowledgments This work is supported by the National Natural Science Foundation of China (Nos.62050073 and 62074134), National Key R&D Program of China (No.2018YFB2200103).

1) T. Pinguet, S. Denton, S. Gloeckner, M. Mack, G. Masini, A. Mekis, S. Pang, M. Peterson, S. Sahni, and P. De Dobbelaere, Proc. IEEE **106**, 2281 (2018).
2) A. E. J. Lim, J. F. Song, Q. Fang, C. Li, X. G. Tu, N. Duan, K. K. Chen, R. P. C. Tern, and T. Y. Liow, IEEE J. Sel. Top. Quantum Electron. **20**, 405 (2014).
3) S. Wirths et al., Nat. Photon. **9**, 88 (2015).
4) S. Zaima, O. Nakatsuka, N. Taoka, M. Kurosawa, W. Takeuchi, and M. Sakashita, Sci. Technol. Adv. Mater. **16**, 043502 (2016).
5) O. Nakatsuka, N. Tsutsui, Y. Shimura, S. Takeuchi, A. Sakai, and S. Zaima, Jpn. J. Appl. Phys. **49**, 04DA10 (2010).
6) K. L. Low, Y. Yang, G. Q. Han, W. J. Fan, and Y. C. Yeo, J. Appl. Phys. **112**, 103715 (2012).
7) S. Gupta, B. Magyari-Kope, Y. Nishi, and K. C. Saraswat, J. Appl. Phys. **113**, 073707 (2013).
8) H. Li, Y. X. Cui, K. Y. Wu, W. K. Tseng, H. H. Cheng, and H. Chen, Appl. Phys. Lett. **102**, 251907 (2013).
9) T. Tsukamoto, N. Hirose, A. Kasamatsu, T. Mimura, T. Matsui, and Y. Suda, Appl. Phys. Lett. **106**, 4366 (2015).
10) H. Li, C. Chang, T. P. Chen, H. H. Cheng, Z. W. Shi, and H. Chen, Appl. Phys. Lett. **105**, 151906 (2014).
11) K. Yu, D. L. Zhang, H. Cong, X. Zhang, Y. Zhao, B. W. Cheng, and C. B. LiIEEE, IEEE 13th Int. Conf. on Group IV Photonics (GFP), 2016, p. 34.
12) F. S. Wan, C. Xu, X. Y. Wang, G. Y. Xu, B. W. Cheng, and C. L. Xue, J. Cryst. Growth **577**, 126399 (2022).
13) M. Oehme, D. Buca, K. Kostecki, S. Wirths, B. Hollander, E. Kasper, and J. Schulze, J. Cryst. Growth **384**, 71 (2013).
14) J. Taraci, J. Tolle, J. Kouvetakis, M. R. McCartney, D. J. Smith, J. Menendez, and M. A. Santana, Appl. Phys. Lett. **78**, 3607 (2001).
15) F. Gencarelli, B. Vincent, L. Souriau, O. Richard, W. Vandervorst, R. Loo, M. Caymax, and M. Heyns, Thin Solid Films **520**, 3211 (2012).
16) C. E. Tsai, F. L. Lu, P. S. Chen, and C. W. Liu, Thin Solid Films **660**, 263 (2018).
17) H. Khelidj, A. Portavoce, M. Bertoglio, M. Descoins, L. Patout, K. Hoummada, A. Hallén, A. Charaï, M. C. Benoudia, and D. Mangelinck, Mater. Today Commun.. **26**, 101915 (2021).
18) J. Yang, H. Hu, Y. Miao, L. Dong, B. Wang, W. Wang, and R. Xuan, Materials (Basel). **12**, 2662 (2019).
19) Y. Nakamura, A. Masada, and M. Ichikawa, Appl. Phys. Lett. **91**, 013109 (2007).
20) Y. Nakamura, A. Masada, S. P. Cho, N. Tanaka, and M. Ichikawa, J. Appl. Phys. **102**, 124302 (2007).
21) H. Okamoto, K. Takita, K. Tsushima, T. Tawara, K. Tateno, G. Zhang, and H. Gotoh, Jpn. J. Appl. Phys. **58**, SDDG09 (2019).
22) L. Zhang, H. Hong, C. Li, S. Chen, W. Huang, J. Wang, and H. Wang, Appl. Phys. Express **12**, 055504 (2019).
23) O. G. Schmidt and K. Eberl, Phys. Rev. B. **61**, 13721 (2000).
24) T. S. Yoon, Z. M. Zhao, J. Liu, Y. H. Xie, D. Y. Ryu, T. P. Russell, H. M. Kim, and K. B. Kim, Appl. Phys. Lett. **89**, 063107 (2006).
25) Y. Nakamura, A. Murayama, R. Watanabe, T. Iyoda, and M. Ichikawa, Nanotechnology **21**, 095305 (2010).
26) P. Alonso-González, M. S. Martín-González, J. Martín-Sánchez, Y. González, and L. González, J. Cryst. Growth **294**, 168 (2006).
27) X. Mei, M. Blumin, D. Kim, Z. Wu, and H. E. Ruda, J. Cryst. Growth **251**, 253 (2003).
28) Y. Huangfu, W. Zhan, X. Hong, X. Fang, G. Ding, and H. Ye, Nanotechnology **24**, 185302 (2013).
29) N. Taoka, G. Capellini, N. von den Driesch, D. Buca, P. Zaumseil, M. A. Schubert, W. M. Klesse, M. Montanari, and T. Schroeder, Appl. Phys. Express **9**, 031201 (2016).
30) W. Dou et al., Opt. Mater. Express **8**, 3220 (2018).
31) T. Tsukamoto, N. Hirose, A. Kasamatsu, T. Mimura, T. Matsui, and Y. Suda, J. Mater. Sci. **50**, 4366 (2015).
32) Y. Lei and W. K. Chim, Chem. Mater. **17**, 580 (2005).
33) A. A. Tonkikh, N. D. Zakharov, A. A. Suvorova, C. Eisenschmidt, J. Schilling, and P. Werner, Cryst. Growth Des. **14**, 1617 (2014).
34) R. Bar, A. K. Katiyar, R. Aluguri, and S. K. Ray, Nanotechnology **28**, 295201 (2017).
35) V. Schlykow et al., Appl. Phys. Lett. **109**, 202102 (2016).